Electronically non-adiabatic H atom scattering from low miller index surfaces of silver

Nils Hertl[$,†,§] Kerstin Krüger[$,‡] and Oliver Bünermann[*,‡,¶]

†*Max-Planck-Institut für Multidisziplinäre Naturwissenschaften, Am Faßberg 11, Göttingen, Germany.*

‡*Institut für Physikalische Chemie, Georg-August-Universität, Tammannstraße 6, Göttingen, Germany.*

¶*International Center for Advanced Studies of Energy Conversion, Göttingen*

§*Current address: Department of Chemistry, University of Warwick, Gibbet Hill Road, CV4 7AL, Coventry, United Kingdom*

E-mail: oliver.buenermann@chemie.uni-goettingen.de

Abstract

Reactivity of a surface depends strongly on the surface structure. To study the influence of surface structure on H atom adsorption, we performed inelastic scattering experiments and complementary electronically non-adiabatic molecular dynamics (MD) simulations for H atoms colliding with the three low Miller index surface facets of silver. Experiment reveals very similar energy loss distributions for all three investigated facets. However, for the (100) facet a dependence on the surface orientation is observed that is absent for the other two facets. The non-adiabatic MD simulations manage to describe the experiments well. Despite the observed insignificant influence of the surface geometry on the energy loss distributions,

[$]NH and KK contributed equally to this paper.

our simulations predict that the capability of the H atoms to penetrate the surface critically depends on the surface structure. The observed crystal orientation dependence of the energy loss distributions in the experiment for Ag(100) cannot be explained with our simulations and we provide a discussion for a better theoretical description of this system to stimulate future computational investigations.

Introduction

Adsorption of atomic and molecular hydrogen on surfaces is the gateway to many important chemical processes in nature. For example, it is well established that molecular hydrogen formation in space cannot occur without the catalytic help of interstellar dust grain surfaces.[1] Dissociative adsorption of molecular hydrogen on metal surfaces gives rise to many hydrogenation reactions that are kinetically hindered in the gas phase. Common examples are hydrogenation of olefines on Raney-Ni, Pd and Pt[2] or the Haber-Bosch process where chemisorbed nitrogen reacts with chemisorbed hydrogen on an iron-based catalyst to form ammonia.[3]

The reactivity of a surface is determined by its structure and in the last decades general trends for the adsorption behaviour of atoms and molecules on metal surfaces have been identified.[4–6] For example, dissociative adsorption of molecules preferably occurs on steps rather than on terraces, because atoms have a lower coordination number which promotes chemisorption. An increase of the sticking probability has been observed when replacing a low Miller index fcc surface by a stepped surface for low-energy molecular beam experiments ranging from simple diatomic molecules, such as H_2, to more complex molecules like methane.[7–12] Nørskov and Hammer quantified this trend by introducing the d-band model,[13,14] stating that a reduced coordination number shifts the centre of the metal's d-bands closer to the Fermi-level and thus promotes binding with atomic or molecular adsorbates.[15,16] However, the capacity of a gaseous particle to remain at a surface strongly

depends on the initial kinetic energy and it is therefore not clear whether this quantitative picture also holds for impinging atoms or molecules with incidence kinetic energies of several eVs. Hence, further studies on the role of the surface structure in the equilibration dynamics of such high-energetic particles are needed. A convenient strategy to scrutinise how the energy flow is influenced by the surface structure is to analyse the energy transfer which takes place during the collision between projectile and substrate. A series of scattering experiments have been performed in which high energetic H atoms were shot onto $fcc(111)$ metal surfaces. In combination with electronically non-adiabatic molecular dynamics (MD) simulations it was demonstrated that the energy transfer from the projectile to the metallic surface is dominated by electronic excitations.[17–23] When the metal surface is exchanged with a noble gas surface, however, the excess energy is completely taken up by the lattice and surface penetration was identified to be the first step in adsorption.[24] Regardless of the recent advance on H atom scattering studies, the role of the surface structure has not been the subject of investigation yet.

In this work, we present the first experimental energy loss distributions of high-energetic H atoms inelastically scattered from three different silver surfaces; Ag(100), Ag(110), and Ag(111). We further provide complementary MD with electronic friction (MDEF) simulations performed on a potential energy surface (PES) based on Effective Medium Theory (EMT).[25–27] This PES, originally fitted to DFT data for H at Ag(111),[19] has proven its worth by accurately reproducing experimental energy loss distribution (ELDs).[21] We demonstrate that this PES can also be applied for MDEF simulations for H/Ag(100) and H/Ag(110) without refitting the parameter set. We find that energy loss distributions obtained for H atom scattering from all three metal surfaces are broad and structureless and show no significant dependence on the surface structure. Although the energy loss distributions obtained for all three facets look very much alike we see that the possibility of subsurface scattering is crucially dependent on the surface geometry. In contrast to the ELDs, we find that the in-plane angular distributions (ADs), computed from simulations with and without

non-adiabatic effects, compare well with each other and to the experimental distributions. Despite having achieved a good overall agreement between experiment and theory, we see subtle differences for one facet and give a discussion of how the theoretical treatment can be improved to achieve an even better agreement to experiment.

Methods

Experimental setup

The H atom scattering experiment is described in detail in Refs. 28,29. Briefly, photodissociation of hydrogen iodide molecules using an excimer laser operating at 248 nm produces a hydrogen atom beam with an incidence translational energy of $E_{\mathrm{kin,i}} = 1.92\,\mathrm{eV}$. The H atoms first pass through two differential pumping chambers before they enter an ultra-high vacuum scattering chamber and collide with a Ag crystal. The crystal is mounted on a 5-axis manipulator allowing the variation of the polar incidence angle θ_{i} with respect to the surface normal. The translational and angular distributions of the scattered H atoms are detected by Rydberg-atom tagging time-of-flight (TOF), where two laser pulses excite the H atoms to a long-lived Rydberg state just below the ionisation limit.[30] The neutral atoms travel 250 mm before they are field-ionised and detected by a multichannel plate (MCP) assembly. A multichannel scaler records the TOF distributions, which we convert to energy distributions applying the appropriate Jacobians. The detector is rotatable in the plane defined by the surface normal and incident H atom beam making it possible to obtain TOF distributions at various final polar scattering angles θ_{f}. The Ag surfaces were cleaned by cycles of Ar^+ ion sputtering and annealing at 873 K. Auger electron spectroscopy (AES) was used to check the cleanliness of the surfaces and low-energy electron diffraction (LEED) validated the correct alignment along the respective surface directions. A recently installed load lock together with a transfer system allows a simple exchange of the different Ag samples on a daily basis.

Potential energy surface

The potential energy surface used for the molecular dynamics simulations is based on Effective Medium Theory[25–27] and an optimal EMT-PES for H/Ag(111) with an RMSE of 147 meV has been published recently.[19] Energy loss distributions calculated from molecular dynamics simulations with electronic friction on this PES were found to be in very good agreement with complementary experiments.[21] Within the framework of EMT, the energy formulae do not contain any surface specific terms which motivated us to test the transferability of the previously used H/Ag(111) PES. This was done by comparing EMT-based interaction energies for H/Ag(100) and H/Ag(110) to energies for the same configurations calculated self-consistently with DFT. This comparison was performed without readjusting the EMT fitting parameters published in Ref. 19.

Electronic structure calculations.

In order to investigate the transferability of the EMT-PES, originally fitted to interaction energies for atomic hydrogen on Ag(111) obtained with DFT,[19] we conducted DFT calculations to acquire interaction energies for H at Ag(100) and Ag(110) for comparison. These calculations were performed with VASP5.3.5[31–34] making use of the PBE functional.[35,36] The electron-core interactions were modelled within the framework of the projector-augmented wave (PAW) approach.[37] The cut-off energy for the plane-wave basis set was set to 400 eV and the partial occupancies were modelled with the method of Methfessel and Paxton ($N = 1$).[38] The smearing width σ was set to 0.1 eV. Both surface facets were modelled as (2×2) slab with six metal layers of which the bottom layer was kept fixed. Periodic boundary conditions were employed in all directions. To prevent interactions between the slab and its periodic images along the surface normal direction, a 15 Å vacuum layer has been placed between the metal slabs. The k-point grid of the Brillouin zone was sampled with a $(4 \times 4 \times 1)$ mesh with the sampling scheme of Monkhorst and Pack.[39] To account for the open-shell nature of atomic hydrogen, spin-polarisation was turned on. A single interaction energy calculation

was considered to be converged when the energy difference between two optimisation steps was smaller than 10^{-5} eV and a structure optimisation was stopped when forces $< 10^{-3}$ eV/Å were reached.

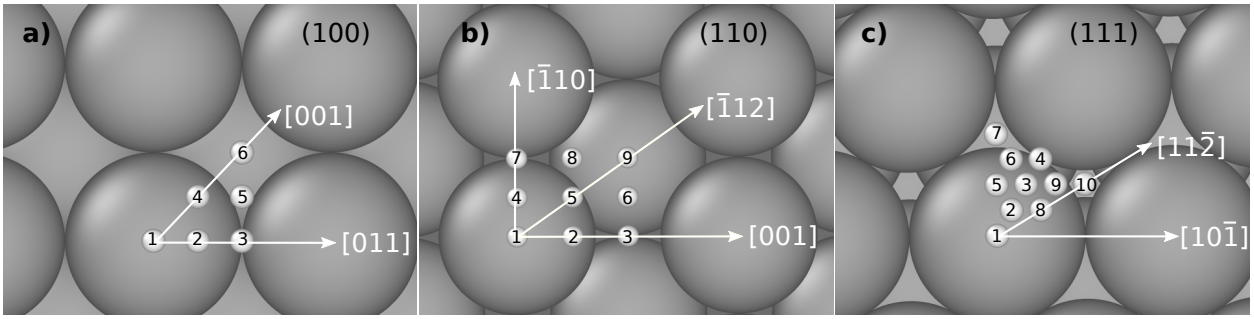

Figure 1: Cuts of the three low-index silver surfaces. The white, numbered spheres indicate the points in the irreducible part of the surface Wigner-Seitz cell which were used for the construction of the 3D grid of DFT energies. The arrows depict the crystallographic directions used in experiment and simulation.

The interaction energies for validation can be categorised into two subsets of data: One subset is a 3D-grid of *ab-initio* energies for H atoms located at the x and y coordinates depicted in Figure 1 and varying z coordinates. The silver atoms remained in their equilibrium lattice positions. The second subset consists of configurations taken from *ab-initio* molecular dynamics (AIMD) trajectories simulating H atom scattering from a 300 K silver surface. In those trajectories, the H atom was placed 6 Å above the surface with the lateral positions chosen randomly. The initial velocities of the H atom are assigned in such a way that they correspond to an initial kinetic energy of 5 eV and a polar incidence angle θ_i equal to 30°. The time step was set to 0.1 fs and the AIMD trajectory was stopped if the H atom was located 6.05 Å above the surface or the simulation time exceeded 1 ps.

Electronically non-adiabatic molecular dynamics simulations

The motion of the H atom is governed by a Langevin equation

$$m\ddot{\boldsymbol{r}} = -\frac{\partial E(\boldsymbol{r},\mathscr{R})}{\partial \boldsymbol{r}} - m\eta_\mathrm{el}(\boldsymbol{r},\mathscr{R})\dot{\boldsymbol{r}} + \boldsymbol{F}_\mathrm{L}(t). \tag{1}$$

Here, m and $\boldsymbol{r}$ are the mass and position of the H atom, respectively. $E(\boldsymbol{r},\mathscr{R})$ labels the potential energy surface which not only depends on the projectile's position, but also on the positions of the metal atoms $\mathscr{R}$. The drag force $-m\eta_{\mathrm{el}}(\boldsymbol{r},\mathscr{R})\dot{\boldsymbol{r}}$ and the random force $\boldsymbol{F}_{\mathrm{L}}(t)$ account for the electronically non-adiabatic effects in the MD simulations. $\eta_{\mathrm{el}}(\boldsymbol{r},\mathscr{R})$ is the friction coefficient which is calculated from the background density provided by the EMT-PES within the framework of the LDFA.[40–42] The utilised mapping function between background density $n_{\mathrm{EMT}}(\boldsymbol{r},\mathscr{R})$ and the friction coefficient $\eta_{\mathrm{el}}(\boldsymbol{r},\mathscr{R})$ is given elsewhere.[18] The importance of the random force $\boldsymbol{F}_{\mathrm{L}}(t)$ for molecular dynamics with electronic friction has been demonstrated recently.[22] Here, $\boldsymbol{F}_{\mathrm{L}}(t)$ is modelled as Gaussian white noise, i.e.

$$\langle \boldsymbol{F}_{\mathrm{L}}(t)\rangle = 0, \tag{2}$$

and the variance being characterised by the second fluctuation dissipation theorem[43]

$$\langle \boldsymbol{F}_{\mathrm{L}}(t)\boldsymbol{F}_{\mathrm{L}}(t')\rangle = 2k_{\mathrm{B}}Tm\eta_{\mathrm{el}}(\boldsymbol{r},\mathscr{R})\delta(t-t')\mathbb{1}. \tag{3}$$

$\mathbb{1}$ represents the 3×3 unity matrix and T corresponds to the surface temperature. The used EMT-PES and the Langevin propagator are implemented into our self-written program, available at a public repository.[44]

In every MD trajectory, the H atom was placed 6 Å above the surface with random lateral positions. The initial velocity components of the H atom were chosen in such a way that they correspond to a defined initial kinetic energy $E_{\mathrm{kin,i}}$, polar angle θ_{i} and crystallographic direction $[hkl]$. The time step Δt was set to 0.1 fs and the trajectory was stopped if the projectile was more than 6.05 Å above the surface or the simulation time exceeded 1 ps. The initial positions and velocities of the silver atoms at a temperature of choice were acquired in the following way: for 100 ps the silver slab was heated with an Anderson thermostat[45] to the chosen temperature and then propagated in an NVE ensemble making use of the velocity-Verlet algorithm.[46,47] Subsequently, an equilibrium trajectory was run for 1 ns and

a snapshot was taken every 1 ps. These 1,000 snapshots contain the equilibrium geometries of the metal atoms along with their velocities corresponding to the desired temperature.

Results and Discussion

Potential energy surfaces

Figure 2 shows the comparison of the EMT-based interaction energies with the DFT validation data. The EMT-PES, originally parameterised to H/Ag(111) DFT data, is capable of describing 1D curves of interaction energies for H/Ag(100) and H/Ag(110) within a good accuracy; the RMSE with respect to the static grid data of H at Ag(100) and Ag(110) is 0.25 eV and 0.27 eV, respectively. We further compare the EMT-PES's capacity to reproduce interaction energies taken from AIMD trajectories of H atom scattering and absorption events where the initial kinetic energy of the projectile was set to be 5 eV. Again, the agreement between the H/Ag EMT-PES and the validation data are good, which can be taken from Figure 3. The overall RMSE with respect to the H/Ag(100) and H/Ag(110) data is 0.20 eV and 0.24 eV, respectively. With 25 atoms in the simulation cell, this corresponds to RMSEs of 8.0 meV/atom and 9.6 meV/atom. Although it is nowadays possible to achieve RMSEs < 1 meV/atom with Neural-Network potentials, it comes at the cost of complexity. A much larger amount of input data is required to train a Neural-Network potential and it also needs to be retrained for every individual metal facet. The EMT-PES does not suffer from these shortcomings: it requires a much smaller number of input data and is transferable between different surface facets. Also, in contrast to Neural-Network potentials, the EMT-PESs provides a full-dimensional background density for the computation of the friction coefficient.

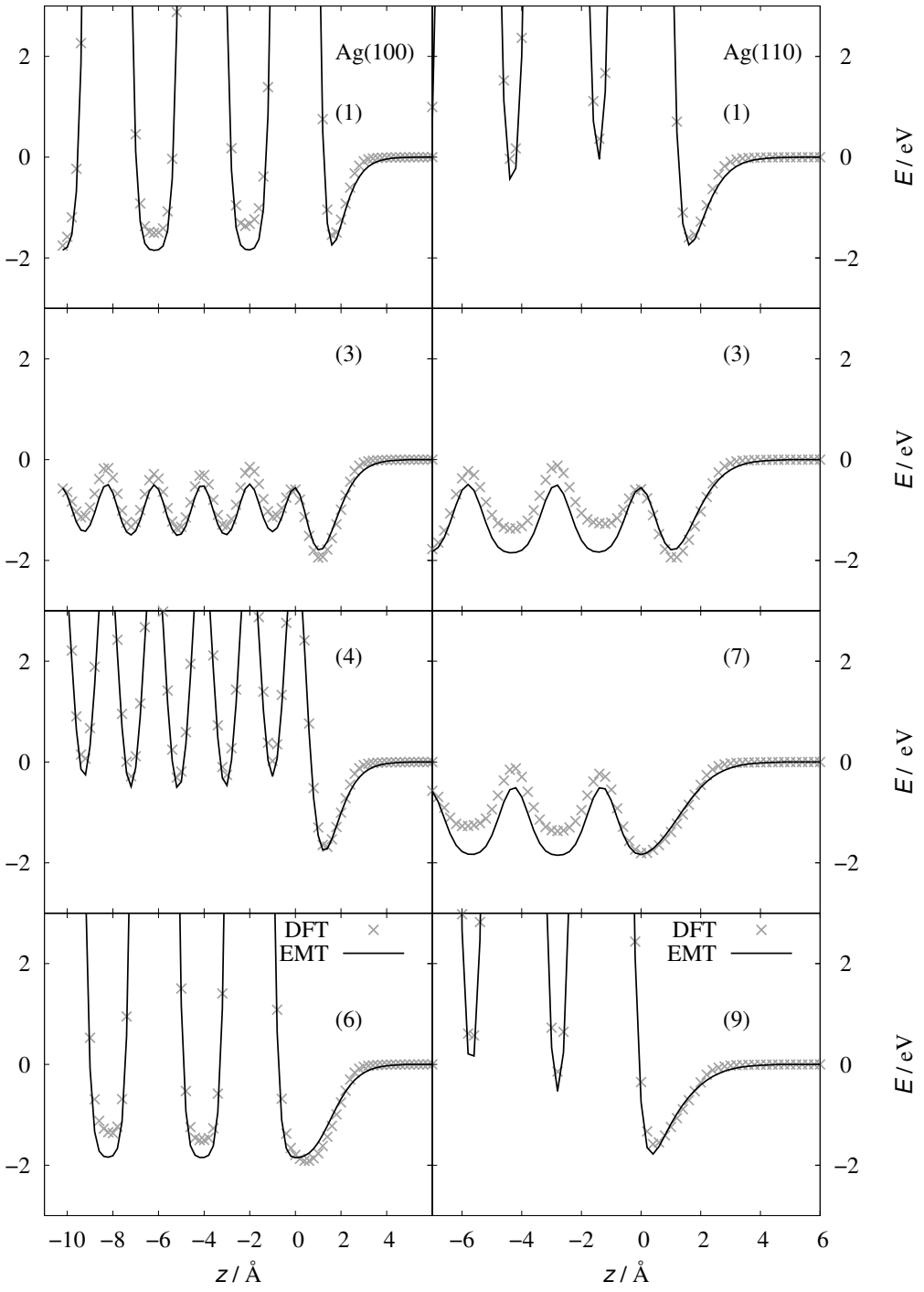

Figure 2: EMT energy dependence on z coordinate of the H-atom at Ag(100) (left panels) and Ag(110) (right panels) shown for several high-symmetry sites—see Figure 1. The grey crosses mark the corresponding DFT energies. The numbers in the individual panels mark the labels of the respective metal facet's high-symmetry sites. Note, the EMT energy expression was fitted to DFT energies for H at Ag(111).

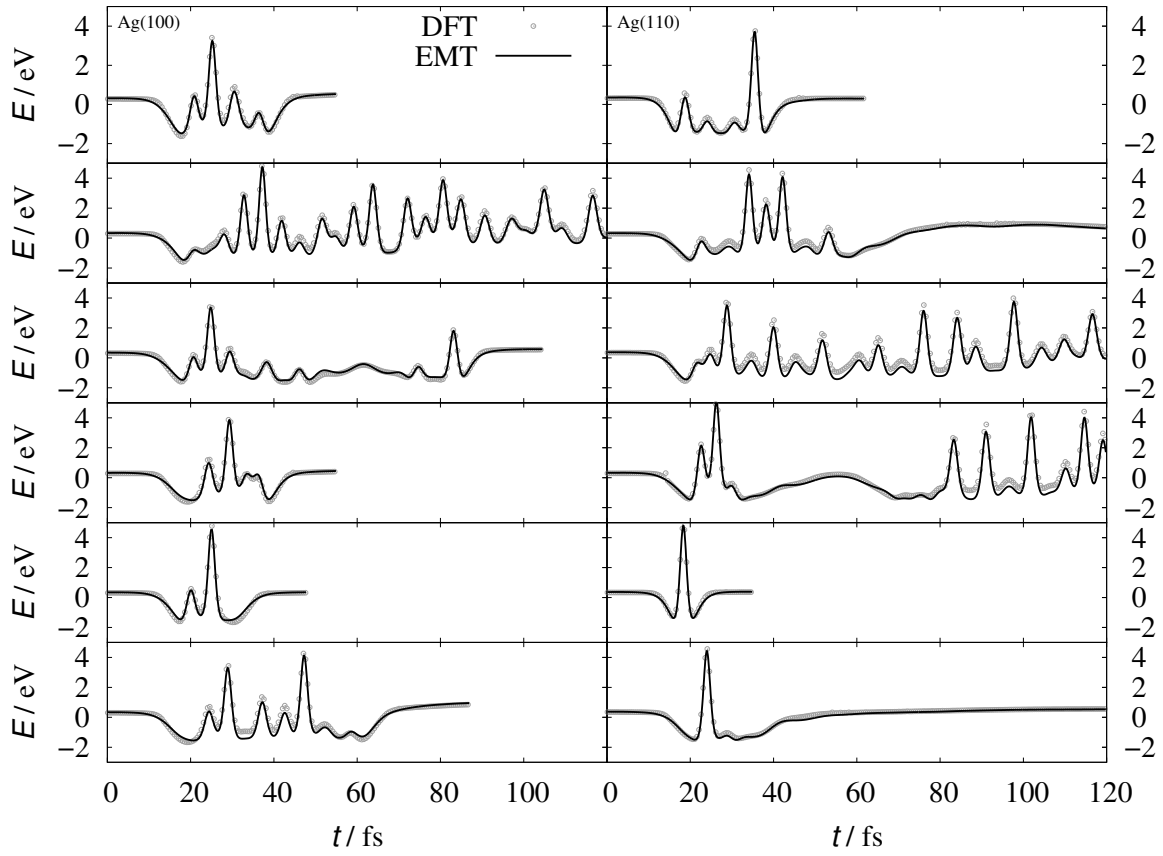

Figure 3: H/Ag(100) (left panels) and H/Ag(110) (right panels) interaction energies calculated for the configurations sampled from AIMD trajectories. The grey circles represent the DFT energies. The black line stands for the EMT-PES.

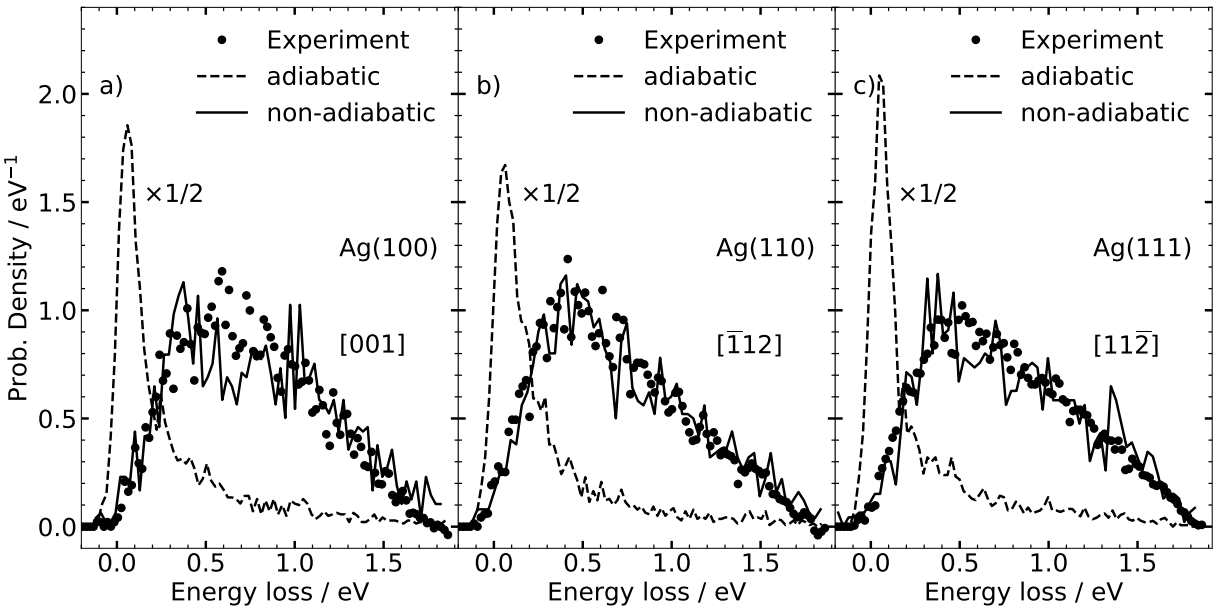

Figure 4: Experimental and theoretical energy loss distributions for H atoms scattered in-plane from three different silver facets with a polar scattering angle $\theta_f = 45°$. The polar incidence angle is $\theta_i = 45°$ and the incidence energy $E_{kin,i}$ is 1.92 eV. The surface temperature is $T_s = 300$ K.

Energy loss distributions

Figure 4 shows the experimentally obtained energy loss distributions (filled circles) as well as the results of adiabatic MD (dashed line) and non-adiabatic MDEF (solid line) simulations for H atoms scattered from the three different low Miller index silver surface facets—Ag(100), Ag(110), and Ag(111). The H atoms approached the surface with an incidence kinetic energy $E_{kin,i}$ of 1.92 eV and a polar incidence angle of 45° with respect to the surface normal. All measurements were performed at room temperature, i.e. 300 K. The initial conditions of the simulations were chosen to agree with the experiment. Calculation of the energy loss distribution involved in-plane scattering trajectories at a final polar angle $\theta_f = 45°$ with a spherical tolerance of 5° to mimic the experimental conditions as accurate as possible. To ensure proper statistical sampling for the energy loss distribution of specular scattered H atoms we launched $1 \cdot 10^6$ trajectories.

The experimentally recorded energy loss distributions for all silver facets are broad and

structureless. The influence of the surface structure on the experimental distributions is weak which is confirmed by theory through the good agreement between the experimental and the calculated energy loss distributions shown in Figure 4. When electronically non-adiabatic effects are omitted, the simulations fail to describe the experimental curves. However, the intensity of the large peak varies from facet to facet, i.e. an influence of the surface structure can be observed in the adiabatic calculations, which will be discussed further below.

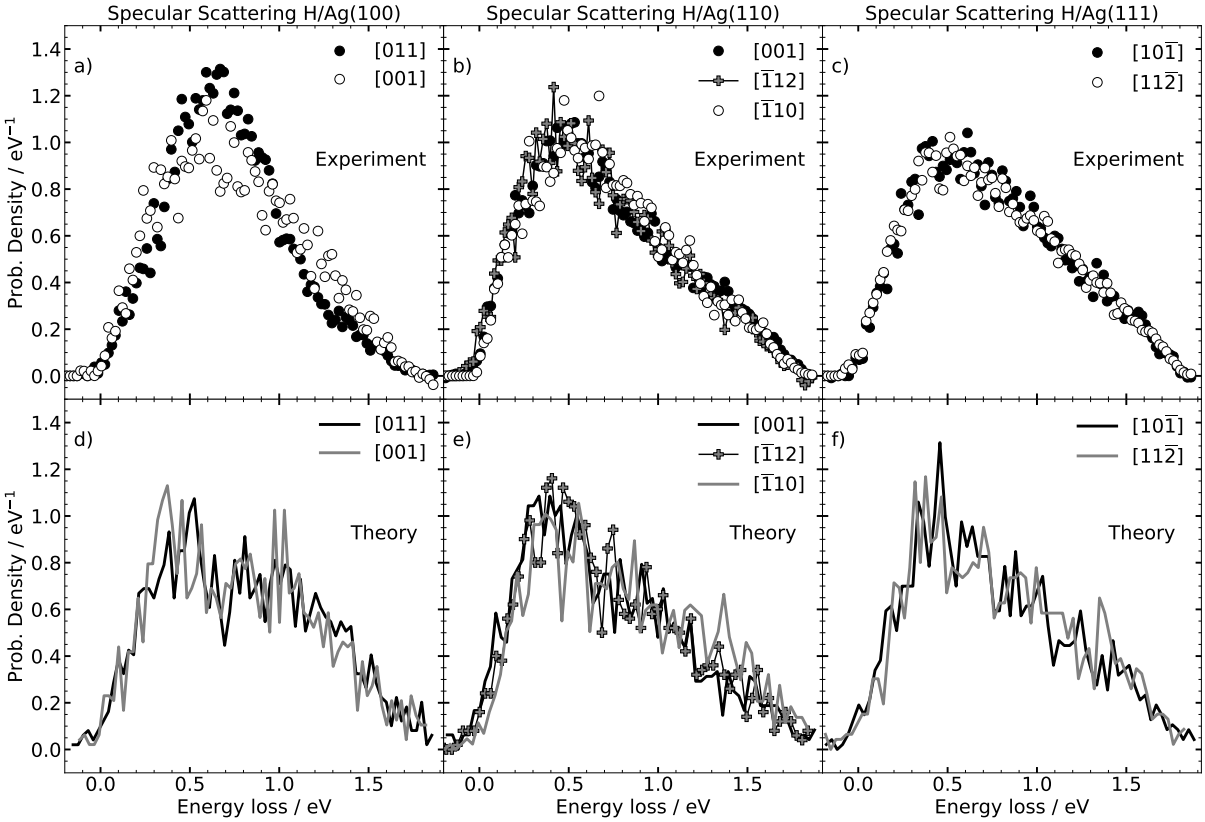

Figure 5: Experimental and theoretical energy loss distributions for H atoms scattered in-plane from three different silver facets with a polar scattering angle $\theta_\mathrm{f} = 45°$ along various crystallographic directions. The polar incidence angle is $\theta_\mathrm{i} = 45°$ and the incidence energy $E_\mathrm{kin,i}$ is 1.92 eV. The surface temperature is $T_\mathrm{s} = 300\,\mathrm{K}$.

Figure 5 shows recorded and calculated energy loss distributions for various crystallographic directions. The other initial conditions are the same as in Figure 4. The appearance of the energy loss distribution is not affected by changing $[hkl]$ for H atom scattering from Ag(111) or Ag(110). Again, theory and experiment are in very good agreement with each

other. For Ag(100), however, the situation is different. Although both theory and experiment yield broad energy loss distributions, ranging from small energy gain up to energy loss close to $E_{\mathrm{kin,i}}$, theoretical simulations predict no influence on the crystallographic direction. In contrast, the experimental curves are slightly influenced by the initial choice of the incidence direction—see panel a) of Figure 5.

We computed the relative mean energy loss $\langle E_{\mathrm{loss}} \rangle / E_{\mathrm{kin,i}}$ from all acquired experimental specular energy loss distribution and found that the scattered H atoms transfer between 35%–41% of their incidence kinetic energy to the metal, which is confirmed by our MDEF simulations. We further see that the mean energy loss does not depend on the surface structure and the crystallographic direction $[hkl]$—see Table S2 in the SI.

Angular distributions

Figure 6 shows the comparison between the measured and calculated angular distributions (AD). The MDEF simulations manage to reproduce the experiment. The ADs of all three Ag facets are broad and without any structure aside from one exception; when H atoms approach the Ag(110) surface along $[\bar{1}12]$, the calculations predict a significant back-scattering channel which is not present when the H atoms impinge along the other incidence directions. Unfortunately, this scattering channel is not accessible through experiment as the geometry of the set-up prevents a detection at such large backwards polar angles.

Surface penetration

Since the experiment can only detect the final energy of the scattered particles, we now analyse the role of surface penetration which has recently been identified to result in higher energy losses.[24,27] The upper panels of Figure 7 show contour plots which provide the number of specular scattering events as a function of energy loss and depth of penetration. A clear correlation between the energy loss and the depth of penetration can be inferred. Note that scattering signal from the third metal layer is negligibly small. The appearance of

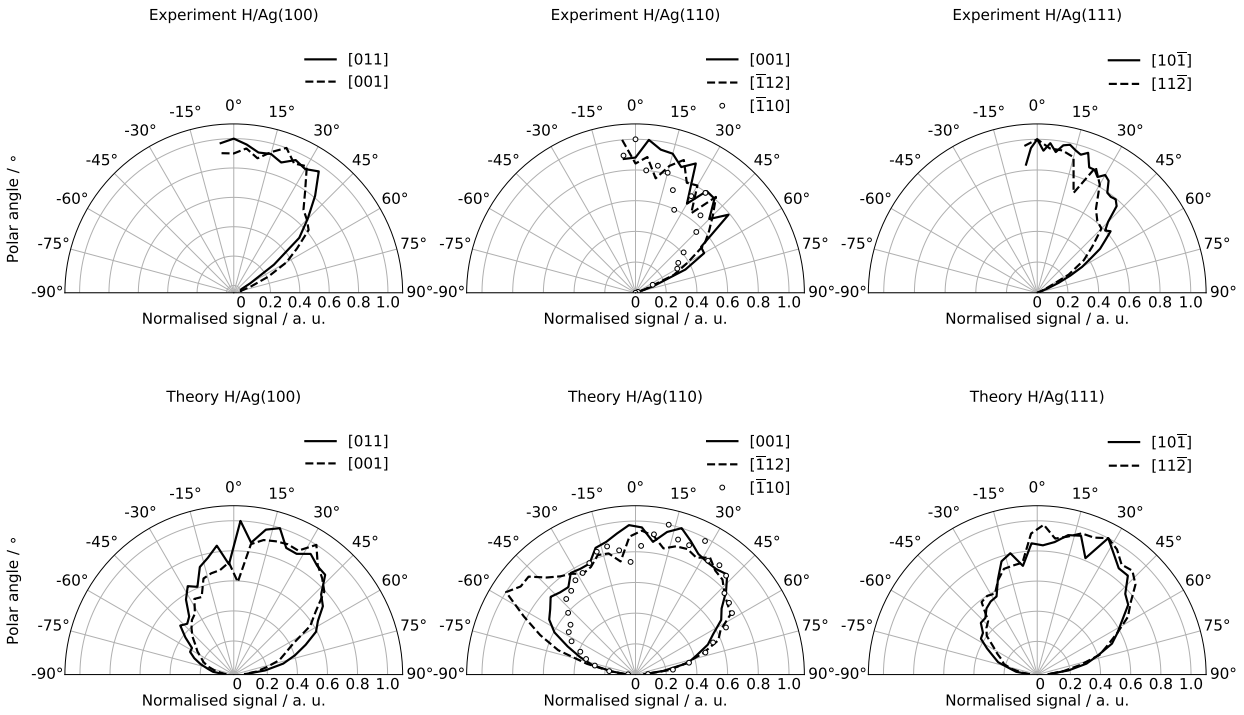

Figure 6: Experimental in-plane angular distributions (upper panels) and their theoretical counterparts (lower panels) for H atoms scattered off Ag(100), Ag(110), and Ag(111). The polar incidence angle corresponds to $\theta_\mathrm{i} = -45°$. The initial kinetic energy is $E_\mathrm{kin,i} = 1.92\,\mathrm{eV}$ and the surface temperature T_s is 300 K. Note that positive and negative polar scattering angles correspond to forward and backward scattering, respectively.

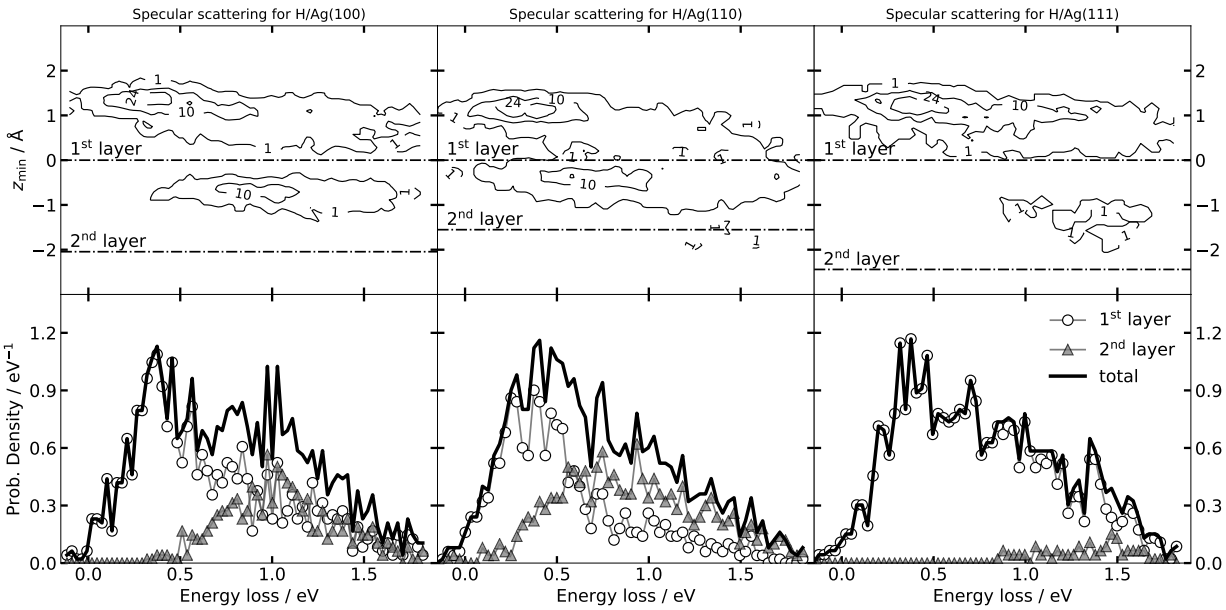

Figure 7: Specular energy loss distributions from Figure 4 decomposed into events where the H atoms scatter either from the first or the second silver layer. Upper panels show 2D histograms where the minimum altitude z_{min} is plotted against the energy loss. The numbers in the contour lines indicate the number of MD trajectories. The dash-dotted lines indicate the location of the first two metal layers. The lower panels resolve the contribution of scattering events of H atoms repelling from the first and second metal layer to the total signal.

the contour plots can be rationalised with the vertical distance d_{12} between surface and subsurface. Smaller distances between the first two layers gives the penetrated projectile less time to excite metal electrons. Ag(110) shows the smallest vertical distance between the first two layers with $d_{12} = 1.55\,\text{Å}$. It is for this small vertical distances why H atoms that advance to the second metal layer show almost the same range of energy losses than projectiles which scatter directly from the top layer. The lower panels show the specular ELDs of Figure 4 decomposed into scattering from the first and second metal layer. Despite the similar appearance of the overall specular energy loss distributions, the underlying scattering dynamics are drastically affected by the surface structure. The $fcc(111)$ surface is a closed-packed surface and thus the chance for H atoms to penetrate the surface twice is extremely low. The contribution of surface penetration events to the ELDs is larger for the other two facets reflecting their smaller planar packing factor ρ_{A} values, which can be inferred from Table S1 in the SI.

Adiabatic vs. non-adiabatic dynamics

By comparing electronically adiabatic and non-adiabatic simulations to the experiments in Figure 4, we demonstrated that electron-hole pair (ehp) excitation are important for all silver surface facets and that a promotion of surface penetration caused by a lower planar packing factor does not alone give rise to broad energy loss distributions observed in the experiment. However, an effect of the surface structure on the energy loss can still be identified in the adiabatic calculations. Like for the energy loss distribution of high-energetic H atoms scattered from Xe(111),[24] the ELDs comprise a large peak, whose energy loss can be well explained with a binary collision model,[48] and a decaying tail towards higher energy losses. Subsurface scattering events contribute to this decaying tail and the lower the planar packing factor of the facet is, the larger gets the contribution of the decaying tail to the overall distribution, i.e. the maximum of the large peak reduces. This can also be inferred from Table S1 in the SI. In fact, surface penetration is dominant, when electronic excitation

are omitted in the simulations for H/Ag(110). In contrast, to the electronically adiabatic simulations, the surface structure only has a minor influence on the shape of the energy loss distributions calculated from the MDEF simulation. This observation can be explained with the large broadening effect the random force $\boldsymbol{F}_{\mathrm{L}}(t)$ casts on the calculated energy loss distributions.[22] The occurrence of scattering from the second metal layer still correlates inversely with the planar packing factor of the facet, but in a reduced manner compared to their adiabatic counterparts, which can be attributed to an increased sticking coefficient S_0, which will be elaborated in the next section.

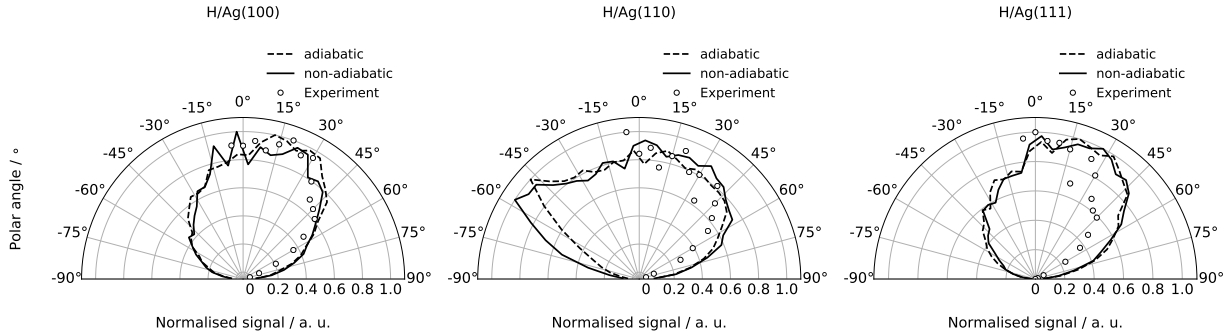

Figure 8: Angular distributions, computed from the same data sets that were used for the calculation of the ELDs in Figure 4, are compared to their experimental counterparts.

We also investigated the influence of non-adiabatic effects on the in-plane angular distributions (AD), see Figure 8. We conclude that ehp excitations, although defining the shape of the ELDs, do not affect the appearance of the ADs. For all three facets, the electronically adiabatic ADs have a more evenly distributed intensity compared to their non-adiabatic counterparts, but the shape of the ADs is maintained and compare well to the experiment.

H atom adsorption

The possibility for the projectile to excite ehps also affects its likelihood to stick which can be taken from Table 1. MDEF simulations predict sticking probabilities larger than 60% and about twice as large as their adiabatic counterparts reflecting the importance of

Table 1: Sticking probability S_0 given in % for adiabatic molecular dynamics (MD) and molecular dynamics with electronic friction (MDEF). The simulation conditions are the same as in Figure 4.

Type	Ag(100)	Ag(110)	Ag(111)
MD	36.6	27.6	37.0
MDEF	70.8	63.1	71.3

ehp excitations in the sticking process. The sticking probability is reduced by ∼10% when H atoms impinge on the Ag(110) surface compared to the other two facets which can be rationalised with the low values for ρ_{A} and d_{12}. We emphasise that this is the first prediction for a surface geometry dependence in the adsorption dynamics of hyperthermal H atoms. Janke *et al.*[18] reported that the majority of adsorbed H atoms on the Au(111) surface underwent surface penetration and migrated back from the subsurface to the surface. We investigate whether this picture holds for the silver surface facets by analysing the minimum altitude of the adsorbed H atoms, see panels a)–c) of Figure 9. For Ag(100) and Ag(110), all adsorbed particles underwent surface penetration. The closed-packed Ag(111) surface, however, shows also adsorption events where the H atoms always remained at the surface layer. The panels d)–f) of Figure 9 compare the final z position z_{fin} of the adsorbed particles with their minimum altitude z_{min} and we see that the H atoms preferably relocate to the surface for all three facets. Therefore, we conclude that this resurfacing mechanism also holds for the other two fcc surface facets, but in an exaggerated manner, as surface penetration is here a prerequisite for adsorption.

Unresolved issues

While our MDEF simulation scheme at the LDFA level provided ELDs in excellent agreement with the experiment for Ag(111) and Ag(110), it predicts a less sensitive dependence on the crystallographic direction in comparison to the experiments done on H/Ag(100)—see Figure 5. The computed in-plane angular distributions are completely characterised by the shape of the PES though and the good agreement with the experiments let us draw the

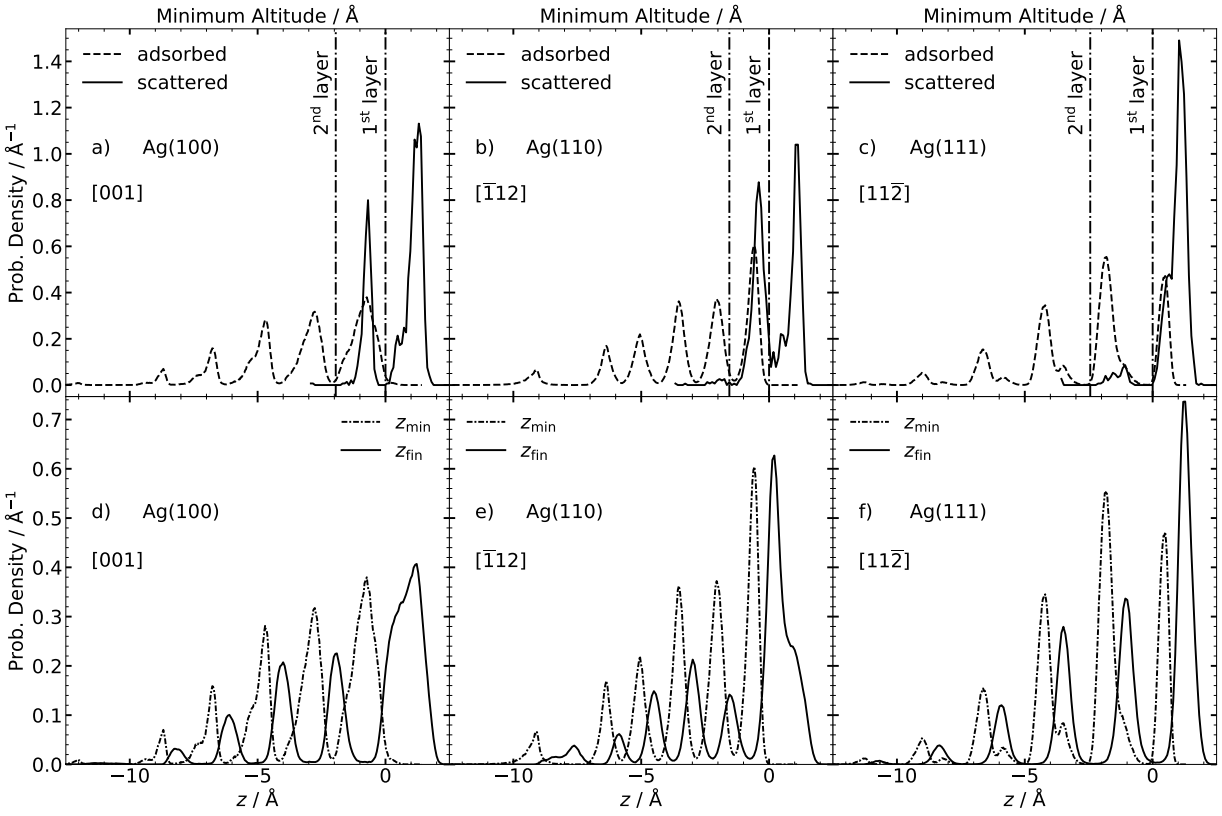

Figure 9: In panel a)–c), the minimum altitude locations $z_{\min}$ of specular scattered and adsorbed H atoms are compared. Panels d)–f) show the probability densities of the minimum altitudes and the final altitudes of the adsorbed H atoms as a function of the z coordinate. Note that $z = 0$ is the location of the surface layer. The initial conditions of the simulations are the same as in Figure 4.

conclusion that the PES is of sufficient accuracy. This allows us to assert that ignoring the tensorial character of the electronic friction in our MDEF simulations is responsible for the absence of the azimuthal angle dependence in the simulations. Askerka *et al.*[49] investigated the diffusion of an adsorbed H atom on Pd(100) with a friction tensor. They found that the individual, diagonal entries of the tensor are different and increase in value when the H atom is located under the surface. Given the substantial contribution of subsurface scattering to the specular energy loss for H/Ag(100), the tensorial treatment of the electronic friction could affect the shape and might describe the azimuthal dependence better than the simple LDFA approach.

In addition, the large broadening effect of the random force $\boldsymbol{F}_{\mathrm{L}}(t)$ disguises subtle differences in the ELDs which may be caused by different travelling directions of the H atom. Thus, to investigate the role of the direction dependence within the framework of LDFA, measurements and calculations at low surface temperatures are required as the broadening effect is predicted to be weak in the low temperature regime.[22] However, at low temperatures nuclear quantum effects might be important. A recently developed stochastic Multi Configurational Time Dependent Hartree approach,[50] which allows the connection of wave-propagation with a bath, might be capable to elucidate the influence of nuclear quantum effects on the scattering dynamics both at room temperature and low temperatures. Our classical, non-adiabatic simulations are in that regard a useful benchmark for this kind of investigation.

Conclusions

In summary, we have reported inelastic H atom scattering experiments from the three silver surfaces Ag(100), Ag(110), and Ag(111) along with complementary molecular dynamics simulations performed on an Effective Medium Theory based PES. The absence of surface dependent terms in the energy expression of EMT allows us to directly use the same PES

for the description of H at Ag(100) and Ag(110), even though the EMT parameters were optimised to input data for H at Ag(111).

The experiments show a weak dependence on the surface geometry which is captured by the MD simulations if electronically non-adiabatic effects are taken into account. This demonstrates that the influence of the surface structure on the energy transfer during the H atom collision with the substrate is of ancillary importance compared to the electronic structure of the material. However, the presence of electronically non-adiabatic effects are not critical for the computation of in-plane angular distributions which we conclude from the good agreement of the MD and MDEF simulations with the experiment.

Similar to the energy loss distribution for the specular scattered H atoms, the sticking probability is more affected by the electronic structure of the surface rather than its geometry. In fact, the probability for an incident particle to stick to the surface decreases approximately by the factor of 2, when ehp excitations are not included in the simulations. In comparison, the sticking probability for Ag(110) is only about 10% smaller compared to the other two facets, Ag(100) and Ag(111), for both MD and MDEF simulations. The details of the adsorption picture, however, are influenced by the surface structure; all adsorbed H atoms on the three silver surfaces follow the penetration-resurfacing mechanism reported by Janke *et al.* in Ref 18. For the more open facets, Ag(100) and Ag(110), adsorbed H atoms need to penetrate the surface in order to stick to it, whereas this is not necessary for the closed-packed Ag(111) facet.

Bottom line, our simulations provide a physical picture to interpret the measurements, but we see a more pronounced dependence on the crystallographic orientation in the experiments for Ag(100). We provided several suggestions to improve the theoretical description to capture this orientation dependence and believe that our analysis of the discrepancies will stimulate future theoretical investigations on this subject.

Supporting Information

Surface Characterisation: Figure S1 shows the low energy electron diffraction (LEED) patterns and Figure S2 the corresponding Auger electron spectra (AES) of the used silver samples.

Planar Packing Factors: Definition of the planar packing factor and its calculation for the three studied surface facets. Table S1 shows the correlation between the planar packing factor and surface penetration observed in the simulations.

Mean energy loss: Table S2 summarises the mean energy losses calculated from the data shown in Figure 1

Acknowledgement

The authors are thankful to Prof. Alec M. Wodtke for continuous support in every aspect of the work. The authors are further indebted to Dr. Alexander Kandratsenka and Prof. Dan Kilillea for fruitful scientific discussions and suggestions of improvement to this manuscript. NH acknowledges financial support from the Max Planck Society Central Funds for this project as well as the Max Planck Institut für Multidisziplinäre Naturwissenschaften. OB and KK acknowledge support from the Deutsche Forschungsgemeinschaft (DFG, German Research Foundation) 217133147/SFB 1073, Project A04.

References

(1) Wakelam, V.; Bron, E.; Cazaux, S.; Dulieu, F.; Gry, C.; Guillard, P.; Habart, E.; Hornekær, L.; Morisset, S.; Nyman, G.; Pirronello, V.; Price, S. D.; Valdivia, V.; Vidali, G.; Watanabe, N. H2 formation on interstellar dust grains: The viewpoints of theory, experiments, models and observations. *Molecular Astrophysics* **2017**, *9*, 1–36.

(2) Brückner, R. *Reaktionsmechanismen*, 3rd ed.; Spektrum Akad. Verl.: Berlin, 2009.

(3) Masel, R. *Principles of adsorption and reaction on solid surfaces*; Wiley-VCH: New-York, 1996; p 501.

(4) Groß, A. *Theoretical surface science: A microscopic perspective*; Springer Verlag: Berlin Heidelberg, 2009.

(5) Bligaard, T.; Nørskov, J. In *Chemical Bonding at Surfaces and Interfaces*, 1st ed.; Nilsson, A., Pettersson, L., Nørskov, J., Eds.; Elsevier: Amsterdam, 2008; pp 255–322.

(6) Luntz, A. In *Chemical Bonding at Surfaces and Interfaces*, 1st ed.; Nilsson, A., Pettersson, L., Nørskov, J., Eds.; Elsevier: Amsterdam, 2008; pp 143–254.

(7) Gee, A.; Hayden, B.; Mormiche, C.; Nunney, T. The role of steps in the dynamics of hydrogen dissociation on Pt (533). *The Journal of Chemical Physics* **2000**, *112*, 7660–7668.

(8) Luntz, A.; Brown, J.; Williams, M. Molecular beam studies of H2 and D2 dissociative chemisorption on Pt (111). *The Journal of chemical physics* **1990**, *93*, 5240–5246.

(9) Groot, I.; Schouten, K.; Kleyn, A.; Juurlink, L. Dynamics of hydrogen dissociation on stepped platinum. *The Journal of chemical physics* **2008**, *129*, 224707.

(10) Groot, I. M.; Kleyn, A. W.; Juurlink, L. B. The energy dependence of the ratio of step and terrace reactivity for H2 dissociation on stepped platinum. *Angewandte Chemie International Edition* **2011**, *50*, 5174–5177.

(11) Migliorini, D.; Chadwick, H.; Nattino, F.; Gutiérrez-González, A.; Dombrowski, E.; High, E. A.; Guo, H.; Utz, A. L.; Jackson, B.; Beck, R. D.; Kroes, G.-J. Surface Reaction Barriometry: Methane Dissociation on Flat and Stepped Transition-Metal Surfaces. *The Journal of Physical Chemistry Letters* **2017**, *8*, 4177–4182.

(12) Chadwick, H.; Guo, H.; Gutiérrez-González, A.; Menzel, J. P.; Jackson, B.; Beck, R. D. Methane dissociation on the steps and terraces of Pt (211) resolved by quantum state and impact site. *The Journal of Chemical Physics* **2018**, *148*, 014701.

(13) Hammer, B.; Nørskov, J. Electronic factors determining the reactivity of metal surfaces. *Surface Science* **1995**, *343*, 211–220.

(14) Hammer, B.; Nørskov, J. K. Why gold is the noblest of all the metals. *Nature* **1995**, *376*, 238–240.

(15) Hammer, B.; Nielsen, O. H.; Nørskov, J. Structure sensitivity in adsorption: CO interaction with stepped and reconstructed Pt surfaces. *Catalysis Letters* **1997**, *46*, 31–35.

(16) Mavrikakis, M.; Hammer, B.; Nørskov, J. K. Effect of strain on the reactivity of metal surfaces. *Physical Review Letters* **1998**, *81*, 2819.

(17) Bünermann, O.; Jiang, H.; Dorenkamp, Y.; Kandratsenka, A.; Janke, S. M.; Auerbach, D. J.; Wodtke, A. M. Electron-hole pair excitation determines the mechanism of hydrogen atom adsorption. *Science* **2015**, *350*, 1346–1349.

(18) Janke, S. M.; Auerbach, D. J.; Wodtke, A. M.; Kandratsenka, A. An accurate full-dimensional potential energy surface for H-Au(111): Importance of nonadiabatic electronic excitation in energy transfer and adsorption. *Journal of Chemical Physics* **2015**, *12*, 124708.

(19) Kammler, M.; Janke, S. M.; Kandratsenka, A.; Wodtke, A. M. Genetic algorithm approach to global optimization of the full-dimensional potential energy surface for hydrogen atom at fcc-metal surfaces. *Chemical Physics Letters* **2017**, *683*, 286–290.

(20) Kandratsenka, A.; Jiang, H.; Dorenkamp, Y.; Janke, S. M.; Kammler, M.; Wodtke, A. M.; Bünermann, O. Unified description of H-atom–induced chemicurrents and inelastic scattering. *Proc. Natl. Acad. Sci. U. S. A.* **2018**, *115*, 680–684.

(21) Dorenkamp, Y.; Jiang, H.; Köckert, H.; Hertl, N.; Kammler, M.; Janke, S. M.; Kandratsenka, A.; Wodtke, A. M.; Bünermann, O. Hydrogen collisions with transition metal surfaces: Universal electronically nonadiabatic adsorption. *J. Chem. Phys.* **2018**, *148*, 034706.

(22) Hertl, N.; Martin-Barrios, R.; Galparsoro, O.; Larrégaray, P.; Auerbach, D. J.; Schwarzer, D.; Wodtke, A. M.; Kandratsenka, A. Random Force in Molecular Dynamics with Electronic Friction. *The Journal of Physical Chemistry C* **2021**, *125*, 14468–14473.

(23) Lecroart, L.; Hertl, N.; Dorenkamp, Y.; Jiang, H.; Kitsopoulos, T. N.; Kandratsenka, A.; Bünermann, O.; Wodtke, A. M. Adsorbate modification of electronic nonadiabaticity: H atom scattering from p(2 × 2) O on Pt(111). *The Journal of Chemical Physics* **2021**, *155*, 034702.

(24) Hertl, N.; Kandratsenka, A.; Bünermann, O.; Wodtke, A. M. Multibounce and Subsurface Scattering of H Atoms Colliding with a van der Waals Solid. *The Journal of Physical Chemistry A* **2021**, *125*, 5745–5752.

(25) Jacobsen, K. W.; Nørskov, J. K.; Puska, M. J. Interactomic interaction in the effective-medium theory. *Physical Review B* **1987**, *35*, 7423–7442.

(26) Jacobsen, K. W.; Stoltze, P.; Nørskov, J. K. A semi-empirical effective medium theory for metals and alloys. *Surface Science* **1996**, *366*, 394–402.

(27) Hertl, N.; Kandratsenka, A.; Wodtke, A. M. Effective medium theory for bcc metals: electronically non-adiabatic H atom scattering in full dimensions. *Phys. Chem. Chem. Phys.* **2022**, *24*, 8738–8748.

(28) Bünermann, O.; Jiang, H.; Dorenkamp, Y.; Auerbach, D. J.; Wodtke, A. M. An ultrahigh vacuum apparatus for H atom scattering from surfaces. *Review of Scientific Instruments* **2018**, *89*, 094101.

(29) Bünermann, O.; Kandratsenka, A.; Wodtke, A. M. Inelastic Scattering of H Atoms from Surfaces. *The Journal of Physical Chemistry A* **2021**, *125*, 3059–3076, PMID: 33779163.

(30) Schnieder, L.; Seekamp-Rahn, K.; Liedeker, F.; Steuwe, H.; Welge, K. H. Hydrogen exchange reaction H + D2 in crossed beams. *Faraday Discuss. Chem. Soc.* **1991**, *91*, 259–269.

(31) Kresse, G.; Furthmüller, J. Efficient iterative schemes for ab initio total-energy calculations using a plane-wave basis set. *Physical Review B* **1996**, *54*, 11169–11186.

(32) Kresse, G.; Furthmüller, J. Efficiency of ab-initio total energy calculations for metals and semiconductors using a plane-wave basis set. *Computational Materials Science* **1996**, *6*, 15–50.

(33) Kresse, G.; Hafner, J. *Ab initio* molecular dynamics for liquid metals. *Physical Review B* **1993**, *47*, 558.

(34) Kresse, G.; Hafner, J. *Ab initio* molecular-dynamics simulation of the liquid-metal–amorphous-semiconductor transition in germanium. *Physical Review B* **1994**, *49*, 14251.

(35) Perdew, J. P.; Burke, K.; Ernzerhof, M. Generalized Gradient Approximation Made Simple. *Physical Review Letters* **1996**, *77*, 3865–3868.

(36) Perdew, J. P.; Burke, K.; Ernzerhof, M. Generalized Gradient Approximation Made Simple. *Physical Review Letters* **1997**, *78*, 1396.

(37) Blöchl, P. E. Projector Augmented-Wave Method. *Phys. Rev. B* **1994**, *50*, 17953–17979.

(38) Methfessel, M.; Paxton, A. T. High-precision sampling for Brillouin-zone integration in metals. *Phys. Rev. B* **1989**, *40*, 3616–3621.

(39) Monkhorst, H. J.; Pack, J. D. Special points for Brillouin-zone integrations. *Physical Review B* **1976**, *13*, 5188–5192.

(40) Li, Y.; Wahnström, G. Nonadiabatic effects in Hydrogen Diffusion in Metals. *Physical Review Lett* **1992**, *68*, 3444–3447.

(41) Li, Y.; Wahnström, G. Molecular-dynamics simulation of hydrogen diffusion in palladium. *Physical Review B* **1992**, *46*, 14528–14542.

(42) Juaristi, J.; Alducin, M.; Díez Muiño, R.; Busnengo, H.; A, S. Role of Electron-Hole Pair Excitations in the Dissociative Adsorption of Diatomic Molecules on Metal Surfaces. *Physical Review Letters* **2008**, *100*, 116102.

(43) Kubo, R.; Toda, M.; Hashitsume, N. *Statistical Physics II*; Springer Verlag: Berlin Heidelberg, 1985.

(44) Auerbach, D. J.; Hertl, N.; Janke, S. M.; Kammler, M.; Kandratsenka, A.; Lecroart, L.; Wille, S. Molecular Dynamics Tian Xia 2 (MDT2): program for simulating the scattering of atoms and molecules from surfaces. Available at https://github.com/akandra/md_tian2. 2021; `https://github.com/akandra/md_tian2.git`.

(45) Andersen, H. C. Molecular dynamics simulations at constant pressure and/or temperature. *J. Chem. Phys.* **1980**, *72*, 2384.

(46) Verlet, L. Computer "Experiments" on Classical Fluids. I. Thermodynamical Properties of Lennard-Jones Molecules. *Physical Review* **1967**, *159*, 98–103.

(47) Verlet, L. Computer "Experiments" on Classical Fluids. II. Equilibrium Correlation Functions. *Physical Review* **1968**, *165*, 201–214.

(48) Grimmelmann, E. K.; Tully, J. C.; Cardillo, M. J. Hard-cube model analysis of gas-surface energy accommodation. *The Journal of Chemical Physics* **1980**, *72*, 1039–1043.

(49) Askerka, M.; Maurer, R. J.; Batista, V. S.; Tully, J. C. Role of Tensorial Electronic Friction in Energy Transfer at Metal Surfaces. *Phys. Rev. Lett.* **2016**, *116*, 217601.

(50) Mandal, S.; Gatti, F.; Bindech, O.; Marquardt, R.; Tremblay, J.-C. Multidimensional stochastic dissipative quantum dynamics using a Lindblad operator. *The Journal of Chemical Physics* **2022**, *156*, 094109.

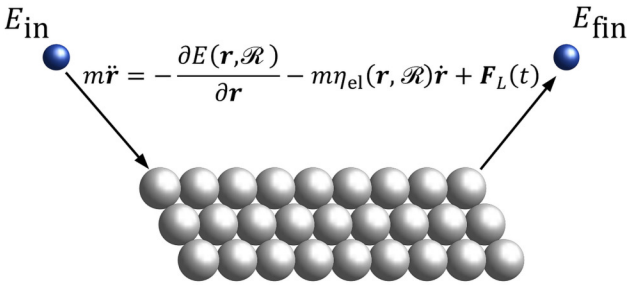

Figure 10: For table of contents only.